Acoustic-phonon emission angle in selectively doped AlGaAs-GaAs-AlGaAs single quantum wells



1994 J. Phys.: Condens. Matter 6 6265

(http://iopscience.iop.org/0953-8984/6/31/026)

J. Phys.: Condens. Matter 6 (1994) 6265–6278. Printed in the UK

# Acoustic-phonon emission angle in selectively doped AlGaAs–GaAs–AlGaAs single quantum wells

W Xu and J Mahanty

Department of Theoretical Physics, Research School of Physical Sciences and Engineering, The Australian National University, Canberra, ACT 0200, Australia

Received 4 January 1994, in final form 6 April 1994

**Abstract.** A detailed theoretical study of the emission rate of the acoustic (AC) phonons is presented for AlGaAs–GaAs–AlGaAs single quantum wells (SQWs). The electron interacting with AC phonons via the deformation potential and piezoelectric coupling is taken into account. We consider the situations where one and two electronic subbands are occupied by electrons, using the results obtained from our self-consistent calculations on the electronic structure. The angle and energy dependences of the AC phonons generated in a GaAs-based two-dimensional electron gas (2DEG) are determined entirely by momentum and energy conservation during the electron–phonon scattering event, in contrast with the process of phonon generation in Si-based structures. Our results show that, in the phonon frequency range $\omega_Q \sim 10^{12}$ Hz, the phonons with higher frequency can be detected at smaller emission angles. The phonons generated through the intersubband scattering processes have a more marked angle dependence and larger emission rate than those generated by intrasubband scattering processes.

## 1. Introduction

With the development and application of the two-dimensional semiconductor systems (2DESs), the investigation of acoustic-phonon emission and scattering by hot electrons in these 2DESs has been of considerable interest over the last decade [1]. The basic difference between phonon emission and scattering by a two-dimensional electron gas (2DEG) and that by the electron gas in 3D results from the following factors: (i) the electronic wavefunctions and density of states in a quantum confined system such as a 2DEG are different from the 3D case [2]; (ii) the interaction between electrons and phonons in the 2DES has different character [3] from the 3D case; and (iii) for a 2DEG the confinement of the electron motion in the $z$-direction implies that the momentum in the $z$-direction will no longer be conserved during an electron–phonon scattering event, which leads [4] to an enhancement of the effective interactions between electrons and phonons and consequently to an enhanced rate of phonon emission and scattering. This has important implications in our understanding of the factors that determine the transport processes involving quantities such as mobility and magnetoresistance [5] and of important phenomena such as the quantum Hall effect [6]. There has been an explosive growth in fabrication of 2D electronic devices using techniques such as MBE and MOCVD. The possibility of tuning and controlling the intensity and the frequency of the emitted phonons in a 2D electronic device, thereby furthering applications in high-frequency devices [7], is the main motivation of this study.

Acoustic- (AC-) phonon emission and scattering by 2D electrons in metal–insulator–semiconductor (MOS) structures [8, 9], GaAs MODFET structures [10], selectively doped Al–GaAs/GaAs heterojunctions [11], and quantum wells [12, 13] has been studied in detail.

0953-8984/94/316265+14$19.50  

The energy and angular distributions of the emitted phonons have also been investigated both theoretically [14, 15] and experimentally [16] in the presence of high magnetic fields applied perpendicular to the interface of the 2D devices. The experimental methods to detect the AC-phonon signal in a 2DES were described in [1] and [17]. The results obtained from the experimental measurements show that (1) the phonon signals detected at low lattice temperatures and relatively low power levels are mainly due to 3D bulk AC phonons; (2) for higher power levels the signal is broadened due to the effects of the longitudinal optic phonons emitted by the 2D electrons; (3) the intensity of the AC-phonon signals depends strongly on the emission angle and on the phonon energy $\hbar\omega_Q$ with $\omega_Q$ being the phonon frequency and $Q$ the phonon wavevector; and (4) the intensity of the phonon signals varies for different sample structures and experimental conditions such as applied fields, gate voltage, etc. Theoretically, the energy and angular distribution of the emitted phonons in a 2DEG can be studied by [8] using the electron–phonon interaction matrix for the 2D system in Fermi's golden rule to obtain the transition rate, which occurs in the Boltzmann equation for phonons, and solving the latter [13].

In this paper we study AC-phonon emission and scattering in a 2DEG in which several electronic subbands are occupied. In such a case we predict a stronger intensity of the phonon signal and a more marked energy and angular dependence of the emitted phonons compared with the situation in which only the lowest subband is occupied. The latter case, in which the AC phonons are generated mainly through electron scattering within the one occupied subband, has received more attention in recent publications than the case we study here. The energy losses from a 2DEG interacting with AC phonons in the case of two-subband occupancy have been studied in detail in [18, 19]. This work was focused on the rate of the *total energy loss* from the 2DEG in AlGaAs/GaAs heterojunctions where the population of electrons in the first exciting subband can normally be achieved by external experimental conditions such as illumination [19, 20]. In this paper we look into the *details* of the emitted AC phonons by studying the angle and energy dependence of the AC-phonon emission in AlGaAs–GaAs–AlGaAs single-quantum-well (SQW) structures where the multi-subband occupation can be achieved by varying the width of the well layer. The results obtained from this study would be valuable for measurements of the phonon signal. As a consequence of multisubband occupancy of electrons, (i) the process of generation of the AC phonons includes the contribution from all the occupied subbands; (ii) the intersubband scattering is of importance for the detected intensity of the phonon signals; (iii) due to different energy-transfer processes between intrasubband and intersubband scattering differences in the energy and angular dependence of the emitted phonon for the different processes can be observed; and (iv) the intersubband scattering brings the possibility of generating higher-frequency AC phonons due to the relatively large separation between different electronic subbands.

The formulas used in the calculations on the electron–phonon interaction in a 2DEG are presented in section 2. In section 3 the AC-phonon emission by 2D electrons in SQW structures will be discussed. The numerical results for the angle and frequency dependence of the emitted phonons in SQW systems are presented and analysed in section 4, and our conclusions are summarized in section 5.

## 2. Electron–acoustic-phonon scattering in a 2DEG

Although the exact distribution of phonon modes in 2DESs such as in the AlGaAs–GaAs–AlGaAs SQW will be complicated due to the presence of the interfaces, we assume that

the phonon modes are like the bulk ones in GaAs. This simplifying assumption, which ignores reflections at the hetero-interfaces, is made because of the structural compatibility of GaAs and AlGaAs, which would not allow a large discontinuity in elastic properties across the interfaces. For this reason, we believe that the trends we obtain in this model will not change substantially, especially for the relatively low-frequency and long-wavelength phonon modes discussed in the present paper, if a more detailed picture of phonon modes including interfacial effects is incorporated into the analysis. Experimentally, the influence of AlGaAs barriers on the phonons emitted in the GaAs wells was also found to be small in [21] where the AC-phonon emission in AlGaAs/GaAs superlattices was studied. For an electron interacting with AC phonons with $\omega_Q \sim 10^{12}$ Hz at low lattice temperatures ($T < 10$ K), the small AC-phonon occupation number $N_Q = 1/(e^{\hbar\omega_Q/k_BT} - 1)$ implies that the influence of absorption of the phonons on scattering is negligible. According to Fermi's golden rule, the transition rate per unit time to scatter an electron from the initial state $|k, n\rangle$ to a state $|k', n'\rangle$, while an AC phonon with energy $\hbar\omega_Q$ is emitted, is given by

$$W^{AC}_{n'n}(k', q_z; k) = \frac{2\pi}{\hbar V}(N_Q + 1)|u^{AC}_{n'n}(Q)|^2\delta_{k'-k,q}\delta(E' - E + \varepsilon_{n'} - \varepsilon_n + \hbar\omega_Q) \tag{1}$$

where $n$ is the index for the $n$th electronic subband with energy $\varepsilon_n$, $k = (k_x, k_y)$ is the electron momentum in the $xy$-plane which is the plane of the 2DEG, $Q = (q, q_z) = (q_x, q_y, q_z)$ is the phonon wavevector, and $V$ is the volume of the sample. Further, $E = \hbar^2k^2/2m^*$ is the kinetic energy for electron motion in the $xy$-plane with $m^*$ the effective electron mass assuming a parabolic band structure, and $|u^{AC}_{n'n}(Q)|^2$ is the square of the electron–AC-phonon interaction matrix element. In equation (1) $\delta_{k'-k,q}$ stands for the conservation of the electron momentum in the $xy$-plane and $\delta(E' - E + \varepsilon_{n'} - \varepsilon_n + \hbar\omega_Q)$ leads to energy conservation in the electronic system; these are depicted in figure 1(a) and (b), respectively.

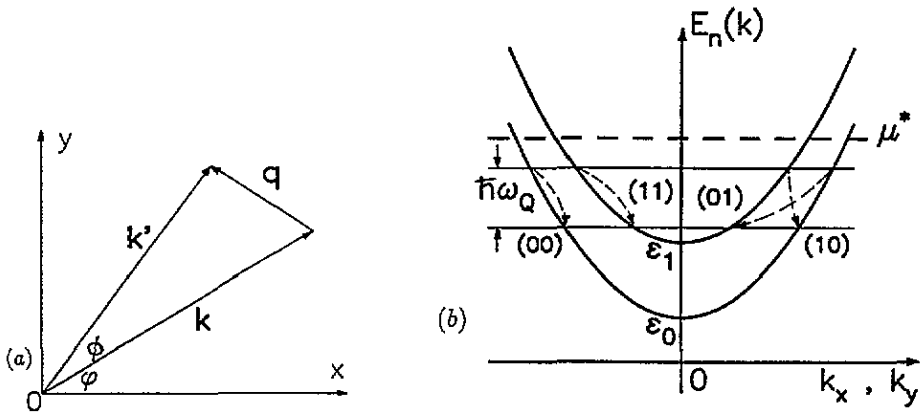


**Figure 1.** (a) Momentum conservation in a 2D electron system in the $xy$-plane. (b) Energy conservation for different phonon emission processes in a 2DEG with two occupied electronic subbands. $E_n(k) = E + \varepsilon_n$ with $E = \hbar^2k^2/2m^*$ is the energy spectrum of the 2D electrons. The condition of energy conservation results in $\varepsilon_q \equiv \hbar^2q^2/2m^* = 2E + a_{n'n}(Q) - 2\sqrt{E[E + a_{n'n}(Q)]}\cos\phi$ and $E' = \hbar^2k'^2/2m^* = E + a_{n'n}(Q)$. In (b), $(ij)$ stands for the process of generating phonons by electron scattering from the $i$th subband to the $j$th subband. $\mu^*$ is the Fermi energy.

The scattering rate per unit time to scatter an electron in the state $|k, n\rangle$, while an AC phonon with energy $\hbar\omega_Q$ is generated, becomes

$$\Gamma_n^{\mathrm{AC}}(q_z, k) = \sum_{n',k'} W_{n'n}^{\mathrm{AC}}(k', q_z; k) f_n(k)[1 - f_{n'}(k')] \tag{2}$$

where the term $f_n(k)[1 - f_{n'}(k')]$, with $f_n(k)$ being the electron momentum-distribution function for the subband $n$, results from scattering in the case of degenerate statistics. The inclusion of the inelastic nature for electron–AC-phonon scattering leads to non-linear electron transport governed by the Boltzmann equation. The solution of this equation gives the electron-distribution function. A popular way to solve the Boltzmann equation in the presence of electron–phonon scattering is through the Monte Carlo method [22]. To simplify matters in this paper we assume that the electron momentum-distribution function can be described by the Fermi–Dirac type of statistical energy-distribution function through [8, 15] $f_n(k) = f_n(E) = [e^{(E+\varepsilon_n-\mu^*)/k_B T_e} + 1]^{-1}$ with $\mu^*$ the chemical potential (or Fermi energy) and $T_e$ the electron temperature. After (i) introducing this electron distribution function into equation (2); (ii) taking account of the momentum and energy conservation shown in figure 1; and (iii) noting that the electron scattering rate due to electron–phonon interactions also gives the rate of generation of phonons with the wavevector $Q$, the emission rate of phonons with the wavevector $Q = (q, q_z)$ is obtained by

$$\Gamma_{q,q_z}^{\mathrm{AC}} = \frac{m^*(N_Q + 1)}{4\pi^2\hbar^3 L_z} \sum_{n,n'} \int_{-\pi}^{\pi} \mathrm{d}\phi \int_{-\pi}^{\pi} \mathrm{d}\varphi \, |u_{n'n}^{\mathrm{AC}}(Q)|^2 f_n(E)[1 - f_n(E - \hbar\omega_Q)] \times \Theta[E + a_{n'n}(Q)] \tag{3}$$

where $\Theta(x) = 0$ $(x < 0), 1$ $(x \geqslant 0)$ is the unit-step function, $a_{n'n}(Q) = \varepsilon_n - \varepsilon_{n'} - \hbar\omega_Q$, and $L_z$ is the sample size in the $z$-direction. The condition of momentum and energy conservation leads to

$$E = \frac{\varepsilon_q - a_{n'n}(Q)\sin^2\phi + \cos\phi\sqrt{\varepsilon_q^2 - a_{n'n}^2(Q)\sin^2\phi}}{2\sin^2\phi} \tag{4}$$

with $\varepsilon_q \equiv \hbar^2 q^2/2m^*$.

In semiconductor materials such as GaAs, both piezoelectric (PE) and deformation potential (DP) interactions play roles in AC-phonon scattering. For GaAs only the longitudinal AC-phonon mode is connected with the deformation potential. The electron-DP–AC-phonon interaction-matrix element is given by [23]

$$|u_{n'n}^{\mathrm{DP}}(Q)|^2 = \frac{\hbar E_{\mathrm{D}}^2 Q}{2\rho v_{\mathrm{sl}}} G_{n'n}(q_z) \tag{5a}$$

with $E_{\mathrm{D}}$ the deformation potential constant, $\rho$ the density of the material, $v_{\mathrm{sl}}$ the longitudinal sound velocity, and $G_{n'n}(q_z) = |\langle n'|e^{-iq_z z}|n\rangle|^2$ the form factor. In a zincblende structure semiconductor material like GaAs, there is only one non-zero independent piezoelectric constant $e_{14} = e_{25} = e_{36}$, and the dielectric constant $\kappa$ and sound velocity are isotropic. For the longitudinal PE-phonon scattering we have [24]

$$|u_{n'n}^{\mathrm{PL}}(Q)|^2 = \frac{32\pi^2\hbar e^2 e_{14}^2}{\kappa^2\rho v_{\mathrm{sl}}} \frac{(3q_x q_y q_z)^2}{Q^7} G_{n'n}(q_z) \tag{5b}$$

and for the transverse PE-phonon scattering we have

$$|u^{\mathrm{PT}}_{n'n}(Q)|^2 = \frac{32\pi^2\hbar e^2 e_{14}^2}{\kappa^2\rho v_{\mathrm{st}}Q^5}\left[q_x^2q_y^2 + q^2q_z^2 - \frac{(3q_xq_yq_z)^2}{Q^2}\right]G_{n'n}(q_z) \tag{5c}$$

with $v_{\mathrm{st}}$ the transverse sound velocity. For electron–phonon scattering the influence of the dynamical screening on the transport properties (e.g., electronic mobility) is relatively weak [25] and we neglect it in the present paper.

Introducing equations (5) for different AC-phonon scatterings into equation (3), we can calculate the acoustic-phonon emission rate. For the longitudinal and transverse modes we obtain, respectively,

$$\Gamma^{\mathrm{AC,L}}_{q,q_z} = \Gamma^{\mathrm{DP}}_{q,q_z} + \Gamma^{\mathrm{PL}}_{q,q_z} \qquad \Gamma^{\mathrm{AC,T}}_{q,q_z} = \Gamma^{\mathrm{PT}}_{q,q_z} \tag{6}$$

where for DP AC phonons

$$\Gamma^{\mathrm{DP}}_{q,q_z} = \frac{m^*}{\hbar^2}\frac{E_{\mathrm{D}}^2 Q}{\pi\rho v_{\mathrm{sl}}L_z}(N_Q+1)\sum_{n,n'}F_{n'n}(q,q_z)G_{n'n}(q_z) \tag{7a}$$

for longitudinal PE AC phonons

$$\Gamma^{\mathrm{PL}}_{q,q_z} = \frac{m^*}{\hbar^2}\frac{36\pi e^2 e_{14}^2}{\kappa^2\rho v_{\mathrm{sl}}L_z}(N_Q+1)\frac{q^4q_z^2}{Q^7}\sum_{n,n'}F_{n'n}(q,q_z)G_{n'n}(q_z) \tag{7b}$$

and for transverse PE AC phonons

$$\Gamma^{\mathrm{PT}}_{q,q_z} = \frac{m^*}{\hbar^2}\frac{4\pi e^2 e_{14}^2}{\kappa^2\rho v_{\mathrm{st}}L_z}(N_Q+1)\frac{q^2(q^4+8q_z^4)}{Q^7}\sum_{n,n'}F_{n'n}(q,q_z)G_{n'n}(q_z). \tag{7c}$$

In equations (7)

$$F_{n'n}(q,q_z) = \Theta[a^2_{n'n}(Q) - \varepsilon_q^2]\int_0^{\sqrt{1-x_0}}\frac{\mathrm{d}x}{\sqrt{2-x^2}}f_n(E)[1-f_n(E-\hbar\omega_Q)] \tag{8}$$

with $x_0 = \sqrt{1-[\varepsilon_q/a_{n'n}(Q)]^2}$ and

$$E = \frac{\varepsilon_q - x^2(2-x^2)a_{n'n}(Q) + (1-x^2)\sqrt{\varepsilon_q^2 - x^2(2-x^2)a^2_{n'n}(Q)}}{2x^2(2-x^2)}.$$

We note that: (1) in equation (8) the term $\Theta[a^2_{n'n}(Q) - \varepsilon_q^2]$ results from momentum and energy conservation, which gives the cut-off of the detected phonon signal in some frequency and angle regimes; (2) the integral term in equation (8) will be affected by the experimental conditions such as lattice temperature and applied electric field and sample parameters such as subband energy, Fermi energy, and electron density, which is the term that determines the intensity of the phonon signal; (3) $G_{n'n}(q_z)$ may be different for different 2DESs; (4) the term $F_{n'n}(q,q_z)G_{n'n}(q_z)$ in equations (7) is the main factor which results in the dependence of the AC-phonon emission rate on the phonon wavevectors $q$ and $q_z$; and (5) $\Gamma^{\mathrm{AC}}_{q,q_z} = \Gamma^{\mathrm{AC}}_{Q,\theta}$ depends on the phonon frequency $\omega_Q$ ($\omega_Q = v_{\mathrm{sl}}Q$ for the longitudinal phonon modes and $\omega_Q = v_{\mathrm{st}}Q$ for the transverse phonon modes in the linear dispersion regime) and on the phonon emission angle $\theta$ defined by figure 2 from which we have $q = Q\sin\theta$ and $q_z = Q\cos\theta$.

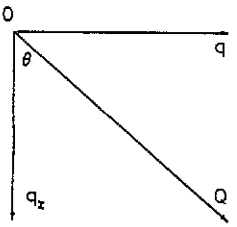


**Figure 2.** The phonon emission angle $\theta$. $q_z = Q\cos\theta$ and $q = Q\sin\theta$.

## 3. Acoustic-phonon emission in AlGaAs–GaAs–AlGaAs SQWs

To calculate the AC-phonon emission rate in 2DESs we need to know the chemical potential $\mu^*$, the energy $\varepsilon_n$, and the wavefunction $\psi_n(z)$ of the electronic subband. Theoretically these quantities can be calculated by solving the Schrödinger equation and the Poisson equation self-consistently for the corresponding 2DEG. Recently we performed [26] a model calculation on the electronic structure of the selectively doped $Al_xGa_{1-x}As$–GaAs–$Al_xGa_{1-x}As$ single quantum wells. In our calculations, the inputs are (i) known material properties, such as $m^*$, $\kappa$, and donor binding energy and (ii) growth parameters, such as concentrations of the acceptor and modulation-doped donor dopants, spacer distances, and Al content. As outputs our calculation gives (1) the confinement potential energy; (2) $E_F$, $\varepsilon_n$, and $\psi_n(z)$; (3) the electron distribution function along the $z$-direction; (4) the depletion lengths; and (5) the total electron density per unit area and the electron density in the occupied electronic subbands. In the present paper we use the results obtained from our self-consistent calculation for the electronic structure in the calculation of the AC-phonon emission rate in the modulation-doped AlGaAs–GaAs–AlGaAs SQW. The advantage of using the SQW structures in the study of AC-phonon emission and scattering is that the occupancy of electrons in the electronic subbands and the position of the energy level of the subbands can be changed by varying the width of the quantum well. When a sufficiently high electric field is applied along the $x$-direction through, e.g., a pulsed electric field [8, 10] experimentally, the 2DEG in the well layer gains energy from the electric field and loses it by emitting the phonons. The emitted AC phonons with the energy $\hbar\omega_Q$ can be detected in certain angular positions. To detect the phonon signal and for guidance in the design of devices it would be valuable to calculate the angle and energy dependences of the phonon emission rate in the 2DES.

The SQW structures used to the study the phonon emission in this paper are depicted in figure 3 where the numerical results are shown for (a) the confinement potential energy and $\varepsilon_n$, and (b) the electron distribution along the direction perpendicular to the interfaces of the SQW for different widths of the quantum well (solid curves $L = 140$ Å, dotted curves $L = 80$ Å). It can be seen that there are two electronic subbands occupied by electrons for the well width $L = 140$ Å and that only the lowest subband is occupied for $L = 80$ Å. In this paper we limit ourselves to the situation with one- or two-electronic-subband occupancy through taking account of well width $L = 80$ Å and 140 Å, with the parameters and electronic properties shown in the caption of figure 3.

With the wavefunctions $\psi_n(z)$ obtained from the self-consistent calculation, we are able to calculate the form factor $G_{mn}(q_z)$ for electron–phonon interaction between subbands $m$ and $n$. The emission-angle dependence of $G_{mn}(q_z)$ is shown in figure 4 for different phonon energies (i.e., for different $Q$) at fixed width of well $L = 140$ Å. At $\theta = \pi/2$ the normalized wavefunctions result in $G_{00}(0) = G_{11}(0) = 1$ and the orthogonality of the electron wavefunctions leads to $G_{01}(0) = G_{10}(0) = 0$. For different phonon energies $\hbar\omega_Q$

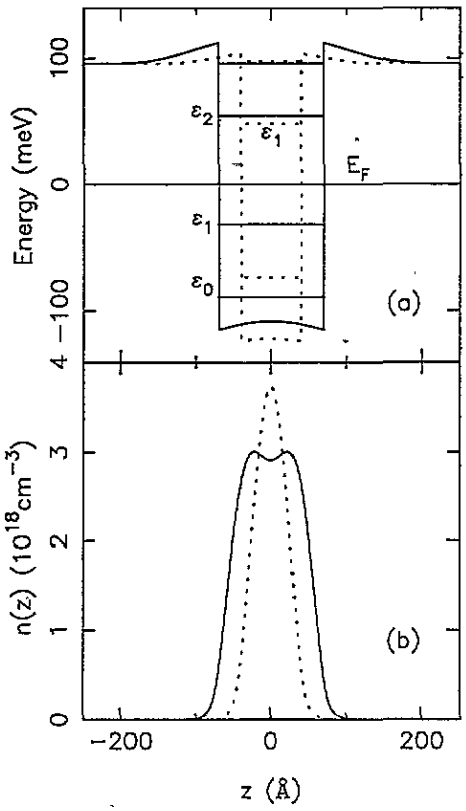


**Figure 3.** The selectively doped $Al_xGa_{1-x}As$–GaAs–$Al_xGa_{1-x}As$ SQW structures used in the calculations in the paper. The results are obtained from the self-consistent calculation in [25] by taking $x = 0.3$, the spacer distances $s_1 = s_2 = 50$ Å, the modulation-doped donor concentration= $2 \times 10^{18}$ cm$^{-3}$, the acceptor concentration= $2 \times 10^{14}$ cm$^{-3}$, and the donor energy= 96 meV. (a) The confinement potential energy and (b) the electron distribution are shown as functions of distance along the direction perpendicular to the interfaces of the SQW for different well widths $L = 140$ Å (solid curves) and $L = 80$ Å (dotted curves). In (a) the energy levels for the electronic subband are also depicted. The electronic properties for $L = 140$ Å ($L = 80$ Å) are (1) the total electron density= $3.38 \times 10^{12}$ cm$^{-2}$ ($2.05 \times 10^{12}$ cm$^{-2}$); (2) the electron densities in the subband $i = 0$, $n_0 = 2.48 \times 10^{12}$ cm$^{-2}$ ($n_0 = 2.05 \times 10^{12}$ cm$^{-2}$) and in the subband $i = 1$, $n_1 = 8.95 \times 10^{11}$ cm$^{-2}$ ($n_1 = 0$); (3) the Fermi energy, measured from the bottom of the conduction band edge in GaAs, $E_F = 115.1$ meV ($E_F = 124.0$ meV); and (4) the depletion lengths, measured from the spacers to the modulation doped regimes, $d_1 = d_2 = 84.5$ Å ($d_1 = d_2 = 51.2$ Å).

the different angle dependences of $G_{mn}(q_z)$ can be observed, which gives the angle and the phonon energy dependences of the AC-phonon emission rate.

In the matter of the angular distribution of the emitted AC phonons, mainly due to deformation potential coupling in a 2DES, the basic differences between Si-based sample structures (e.g., an Si-MOS structure) and GaAs-based ones (e.g., AlGaAs–GaAs–AlGaAs SQWs) are (1) for an Si-based 2DEG the angle dependence is believed [8, 15] to be induced mainly by the ellipsoidal conduction band structure which leads to an extra angle-dependent factor $\chi_l(\theta) = (1 - D\cos^2\theta)^2$ (with $D = -E_U/E_D$, $E_D$ and $E_U$ being the deformation potential constants) for longitudinal modes and $\chi_t(\theta) = \cos^2\theta \sin^2\theta$ for transverse modes;

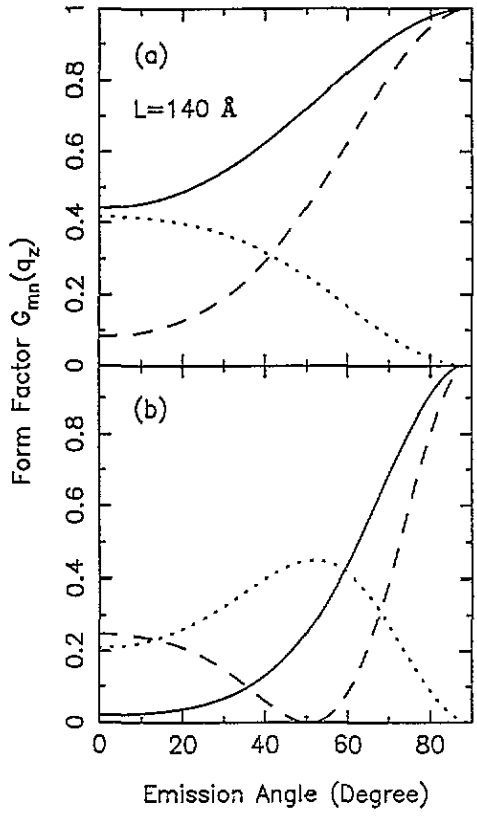


**Figure 4.** The form factor $G_{mn}(q_z = Q\cos\theta) = |\int_{-\infty}^{\infty} dz\ \psi_m^*(z)\psi_n(z)e^{-iq_z z}|^2$: $m = n = 0$ (solid curves); $m = n = 1$ (dashed curves); and $G_{01}(q_z) = G_{10}(q_z)$ (dotted curves), as a function of phonon emission angle $\theta$ for different phonon energies: (a) $\hbar\omega_Q = 1$ meV and (b) 2 meV. The phonon wavevectors for the longitudinal modes are $Q = 2.87 \times 10^{-2}$ Å$^{-1}$ and $5.75 \times 10^{-2}$ Å$^{-1}$, respectively.

(2) for a GaAs-based 2DEG, the angle dependence of the emitted AC phonons is caused entirely by the momentum and energy conservation during the electron–phonon scattering event; and (3) in an Si-based 2DEG the transverse mode of the DP AC phonon can be observed in contrast with the GaAs-based structure, where the transverse mode of the AC phonon can only be observed through piezoelectric coupling.

## 4. Numerical results and discussion

Our calculations are performed for AlGaAs–GaAs–AlGaAs SQW structures, and the material parameters for GaAs are as follows: the effective mass $m^* = 0.0665m_e$ with $m_e$ the electron rest mass, the dielectric constant $\kappa = 12.9$, the material density $\rho = 5.37$ g cm$^{-3}$, the longitudinal sound velocity $v_{sl} = 5.29 \times 10^5$ cm s$^{-1}$, the transverse sound velocity $v_{st} = 2.48 \times 10^5$ cm s$^{-1}$, the piezoelectric constant [27] $e_{14} = 1.41 \times 10^7$ V cm$^{-1}$, and the deformation potential constant [28, 29] $E_D = 11$ eV which leads to a good agreement between the results obtained from theoretical calculations and experimental measurements in [28] by Leadley *et al* for heterojunctions. The SQW sample parameters and electronic

properties are shown in the caption of figure 3. Further, we take the sample size in the $z$-direction to be $L_z = 1000$ Å.

AC-phonon emission by a heated 2DEG implies that the electron temperature $T_e$ is larger than the lattice temperature. It is not easy to determine $T_e$ since it involves non-linear electron transport and depends strongly on the applied electric field and on the electron interacting with both phonons and impurities. Experimentally, $T_e$ can be measured from the amplitude of the Shubnikov–de Haas oscillations [18, 19, 29] and from the photoluminescence spectra [30]. Theoretically, $T_e$ can be calculated by using Monte Carlo simulation [31] and by solving the momentum and energy balance equations [22]. The value of the electron temperature mainly affects the intensity of the phonon signal. To demonstrate the angle dependence of the AC-phonon emission rate and for the sake of simplicity, in this paper we take $T_e$ as a fitting parameter and use $T_e = 15$ K in the calculations.

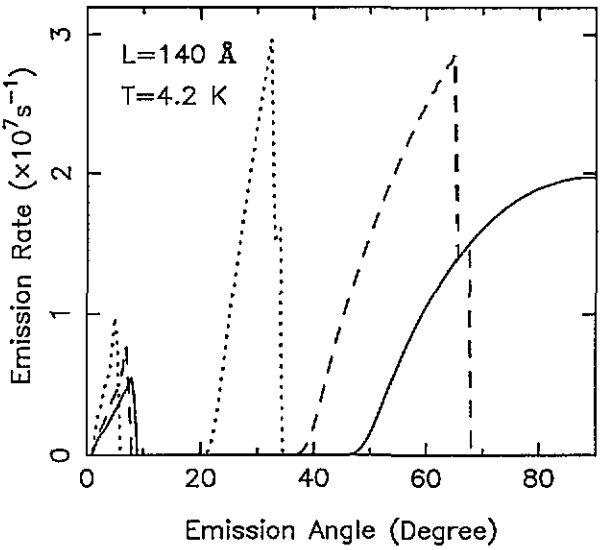


**Figure 5.** The emission-angle dependence of the emission rate for the longitudinal acoustic phonons in the case with two-electronic-subband occupation in an AlGaAs–GaAs–AlGaAs single quantum well with $L = 140$ Å (see figure 3) at lattice temperature $T = 4.2$ K. The results are shown for the phonon energy $\hbar\omega_Q = 1$ meV ($\omega_Q = 1.52 \times 10^{12}$ Hz, solid curves), 1.2 meV ($\omega_Q = 1.82 \times 10^{12}$ Hz, dashed curves), and 2 meV ($\omega_Q = 3.04 \times 10^{12}$ Hz, dotted curves).

In figure 5 the longitudinal AC-phonon emission rate is plotted as a function of emission angle for different phonon frequencies at fixed well width $L = 140$ Å and lattice temperature $T = 4.2$ K. When two electronic subbands are occupied by electrons two peaks for the emission rate can be observed: (i) in the smaller-emission-angle regime the peak corresponds to the intrasubband scattering (i.e. the scattering from subband 0 to 0 and from 1 to 1), and (ii) in the larger-angle regime the peak concerns the intersubband interaction (i.e., for scattering from subband 0 to 1 and from 1 to 0), which is shown in figure 7. For the case of two-subband occupation, the term $\Theta[a^2_{n'n}(Q) - \varepsilon^2_q]$ in equation (8) results in different cut-offs in the emission rates for different phonon frequencies and phonon generation processes. With decreasing phonon frequency (i.e., decreasing phonon energy), (1) the position of the peak for the intersubband scattering moves markedly to the larger-angle regime; (2) the position of the peak for intrasubband scattering shifts slightly to a larger angle; (3) the

peaks are broadened; and (4) the amplitude of the peak decreases. Our numerical results presented in figure 5 show that (i) the rate of generation of the AC phonons through the process of intersubband interaction is larger than that through the intrasubband scattering process; (ii) the signal for a smaller phonon energy can be detected at a larger angle; and (iii) for the case of two-subband occupancy the phonons with the larger energy will have the larger signal intensity.

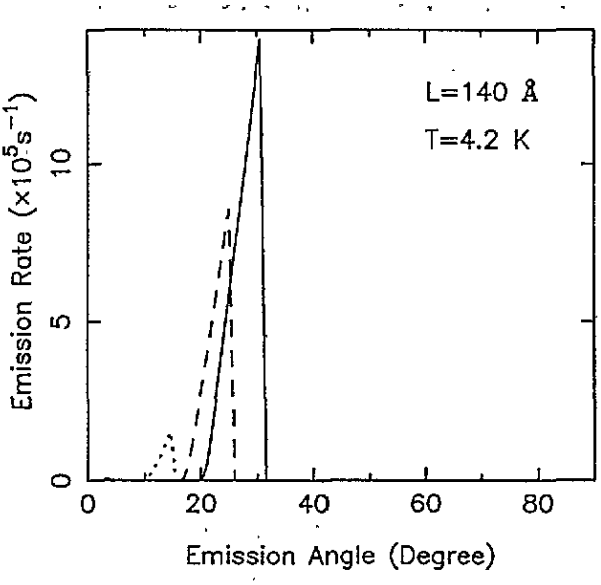


**Figure 6.** The emission-angle dependence of the emission rate for the transverse acoustic phonons. The parameters and the line marks are same as in figure 5. The contributions from intrasubband scattering processes are very small.

The transverse AC-phonon emission rate as a function of emission angle for different phonon frequencies is shown in figure 6 for $L = 140$ Å and $T = 4.2$ K. We note that (1) for the same phonon energy the emission rate of the transverse AC phonons is much smaller than that of the longitudinal phonons; (2) the same phonon energy results in different phonon wavevectors $Q$ for the longitudinal and transverse branches because of different sound velocities; and (3) the generation rate of the transverse AC phonons through the intersubband scattering process is much larger than that through the intrasubband scattering. With decreasing phonon energy the position of the peak moves to the larger-angle regime, but the increase in the amplitude of the peak differs from that for the longitudinal modes shown in figure 5.

In figure 7 we show the contribution to the phonon emission rate from different subband scattering processes for (a) the DP AC phonons and (b) the longitudinal PE AC phonons. It can be seen that (1) the emission rate of the DP AC phonons is much larger than that of the PE AC phonons, which implies that the DP AC phonon is of greater importance in the process of AC-phonon generation in the AlGaAs–GaAs–AlGaAs SQW structures; (2) the generation of the longitudinal PE phonons is mainly through the intersubband scattering process; (3) the process of emission of the AC phonons through scattering from subband 0 to subband 1 (dotted curves) has a slightly different angle dependence from that through scattering from subband 1 to 0 (dashed curves) (the slightly different cut-off in emission rates between

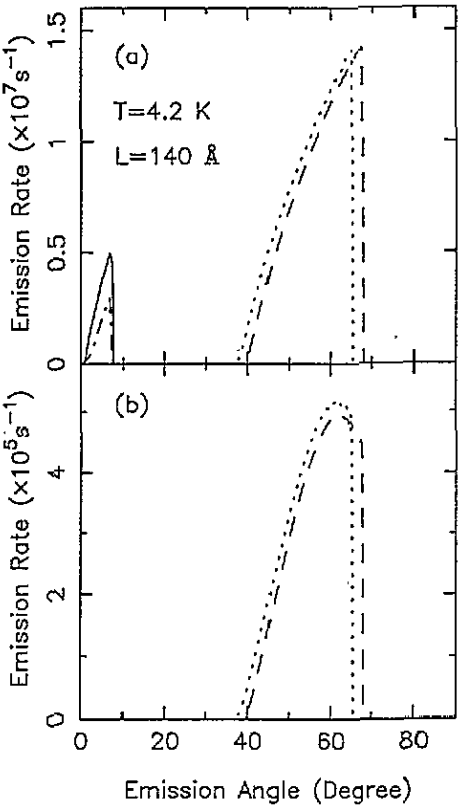


**Figure 7.** The contribution from different subband scattering processes (0 → 0, dashed–dotted curves; 1 → 1, solid curves; 0 → 1, dashed curves; and 1 → 0, dotted curves) to the emission rate of (a) the deformation potential acoustic phonons and (b) the longitudinal piezoelectric phonons. The parameters are taken as the same as in figure 5. The numerical results for the longitudinal piezoelectric phonon emission rate induced by the intrasubband scattering processes are very small.

scattering from 0 → 1 and from 1 → 0 is due to the different processes of energy transfer shown in figure 1(b) and in equation (8): $a_{10}(Q) \neq a_{01}(Q)$); and (4) the phonon emission rate induced by intrasubband scattering in subband 1 (solid curve) is larger than that in subband 0 (dashed–dotted curve).

The angle dependence of the longitudinal AC-phonon emission rate is plotted in figure 8 for different phonon energies under the situation where only the lowest electronic subband is populated by electrons. In this case, the contribution to $\Gamma^{AC}_{Q,\theta}$ from intersubband scattering processes is small, and the total phonon emission rate is smaller than that in the situation with two-subband occupation (see figure 5). With decreasing phonon energy (1) the position of the peak moves to the larger-angle regime; (2) the peak is broadened; and (3) the amplitude of the peak first increases and then decreases. Our theoretical results for the case with only one-subband occupation (shown in figure 8) are consistent with those obtained in [8] for Si-MOS structures. In the theoretical study of [8], the AC-phonon intensity (the summation of phonon emission rate) as a function of phonon energy was studied for different emission angles.

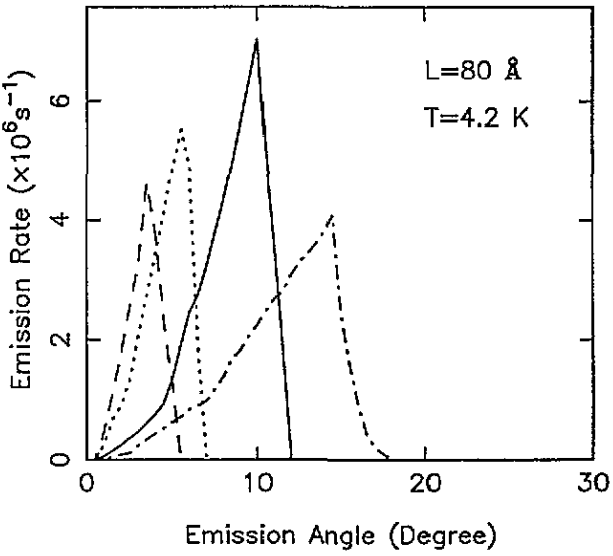


**Figure 8.** The emission-angle dependence of the longitudinal acoustic-phonon emission rate in the case with only one-electronic-subband occupation in an AlGaAs–GaAs–AlGaAs single quantum well with $L = 80$ Å (see figure 3) at lattice temperature $T = 4.2$ K. The results are presented for the phonon energy $\hbar\omega_Q = 0.2$ meV ($\omega_Q = 3.04 \times 10^{11}$ Hz, dashed–dotted curve), 0.5 meV ($\omega_Q = 7.60 \times 10^{11}$ Hz, solid curve), 1.5 meV ($\omega_Q = 2.28 \times 10^{12}$ Hz, dotted curve), and 2.5 meV ($\omega_Q = 3.80 \times 10^{12}$ Hz, dashed curve).

## 5. Summary and conclusions

This theoretical study of the acoustic-phonon emission and scattering by hot electrons in the selectively doped AlGaAs–GaAs–AlGaAs single-quantum-well structures is based on the following model. The electrons in the well interact with AC phonons through deformation potential and piezoelectric coupling. The electronic properties used in the calculations, such as the energy and the wavefunction of the electronic subbands and the Fermi energy, were obtained from the self-consistent calculations of the electronic structure in the SQW. We studied the AC-phonon emission and scattering for the case of one- and two-electronic-subband occupancy. Our conclusions are summarized as follows.

In AlGaAs–GaAs–AlGaAs SQWs with the parabolic band structure of the 2DEG in GaAs, the dependences of the AC-phonon emission rate on the phonon energy and the emission angle are caused entirely by momentum and energy conservation during the electron–phonon scattering event. This differs from the phonon emission and scattering in an Si-based 2DEG (e.g., in Si-MOS structures) in which the ellipsoidal band structure results in an additional emission-angle-dependent factor.

In the selectively doped AlGaAs–GaAs–AlGaAs SQW structure, the occupancy of electrons in the electronic subbands, the energy levels, and the energy separation between different subbands can be tuned by varying the width of the quantum well, thereby bringing in the possibility of generating AC phonons in the desirable phonon frequency regime. As a consequence of several electronic subbands being populated in such a 2DEG, the AC phonons generated through intersubband electron–phonon interaction are of importance in producing the detected phonon signal.

When two electronic subbands are occupied in an SQW, two peaks in the longitudinal

phonon emission rate against the emission angle can be observed. The one with the smaller (larger) intensity and appearing in the smaller- (larger-) emission-angle regime is induced by the intrasubband (intersubband) scattering processes. The decrease in phonon frequency in the range $\omega_Q \sim 10^{12}$ Hz leads to broadening of the peaks and their movement to the larger-angle regime, while the amplitude of the peaks decreases.

In a GaAs-based 2DEG the transverse mode of the AC-phonon can only be generated via piezoelectric coupling. For the case with two-subband occupation in an SQW, the transverse AC phonons are emitted mainly through the intersubband scattering processes. We predict that (1) the intensity of the transverse AC-phonon signal will be relatively weaker than that of the longitudinal mode; (2) in the frequency range $\omega_Q \sim 10^{12}$ Hz the emitted transverse phonons with smaller energies will have stronger signal intensities; and (3) the emitted transverse AC phonons with a lower energy can be detected at a larger emission angle.

In the SQW with only the lowest electronic subband occupied by the electrons, the AC phonons are mainly generated through the process of electron–phonon interaction within this subband. The phonon emission rate is smaller than that in the case with two electronic subbands occupied by electrons. With decreasing phonon frequency, (i) the peak in the emission rate against the emission angle will be broadened and move to a smaller emission angle, and (ii) the emission rate first increases and then decreases. Our numerical results for the case with only one-subband population agree with those shown in [8].

## Acknowledgments

*This research has been carried out on behalf of the Harry Triguboff AM Research Syndicate.* Discussions with Dr M P Das and Dr C Jagadish are gratefully acknowledged. Our special thanks go to Dr T Kent (University of Nottingham, UK) for helpful discussions and useful suggestions.

## References

[1] Challis L J, Kent A J and Rampton V W 1990 *Semicond. Sci. Technol.* **5** 1179
Challis L J 1992 *Low-Dimensional Semiconductor Structures* ed P N Butcher *et al* (New York: Plenum)
[2] Ando T, Fowler A B and Stern 1982 *Rev. Mod. Phys.* **54** 437
[3] Price J P 1982 *Surf. Sci.* **113** 199
[4] Wu X G, Peeters F M and Devreese J T 1985 *Phys. Rev.* B **31** 3420; 1986 *Phys. Status Solidi* b **133** 229
[5] Laedley D R, Nicholas R J, Xu W, Peeters F M, Devreese J T, Singleton J, Perenboom J A A J, van Bockstal L, Herlach F, Foxon C T and Harris J J 1993 *Phys. Rev.* B **48** 5457
[6] Dietzel F, Dietsche W and Ploog K 1993 *Phys. Rev.* B **48** 4713
[7] White R M 1972 *Topics in Solid State and Quantum Electronics* ed W D Hershberger (New York: Wiley)
[8] Rothenfusser M, Köster L and Dietsche W 1986 *Phys. Rev.* B **34** 5518
[9] Kent A J, Hardy G A, Hawker P, Rampton V W, Newton M I, Russell P A and Challis L J 1988 *Phys. Rev. Lett.* **61** 180
[10] Wigmore J K, Erol M, Sahraoui-Tahar M, Wilkinson C D W, Davies J H and Stanley C 1991 *Semicond. Sci. Technol.* **6** 837
[11] Wigmore J K, Erol M, Sahraoui-Tahar M, Ari M, Wilkinson C D W, Davies J H, Holland M and Stanley C 1993 *Semicond. Sci. Technol.* **8** 322
Hawker P, Kent A J, Hughes O H and Challis L J 1992 *Semicond. Sci. Technol.* **7** B29
[12] Greipel K and Rössler U 1992 *Semicond. Sci. Technol.* **7** 487
[13] Vasko F T, Balev G and Vasilopoulos P 1993 *Phys. Rev.* B **47** 16 433
[14] Benedict K A 1991 *J. Phys.: Condens. Matter* **3** 1279; 1992 *J. Phys.: Condens. Matter* **4** L371
Badalian S M and Levinson Y B 1991 *Phys. Lett.* **155A** 200
Fal'ko V I and Iordanskii S V 1992 *J. Phys.: Condens. Matter* **4** 9201

[15] Toombs G A, Sheard F W, Neilson D and Challis L J 1987 *Solid State Commun.* **64** 577
[16] Kent A J, Rampton V W, Newton M I, Carter P J A, Hardy G A, Hawker P, Russell P A and Challis L J 1988 *Surf. Sci.* **196** 410
Hawker P, Kent A J, Challis L J, Henini M and Hughes O H 1989 *J. Phys.: Condens. Matter* **1** 1153
Rampton V W, Newton M I, Carter P J A, Henini M, Hughes O H, Heath M, Davies M, Challis L J and Kent A J 1990 *Acta Phys. Slovakia* **40** 5
[17] Giuliani A and Sanguinetti S 1993 *Mater. Sci. Eng.* R **11** 1
[18] Kreshchuk A M, Martisov M Yu, Polyanskaya T A, Sabel'ev I G, Saidashev I I, Shik A Ya and Shmartsev V Yu 1988 *Sov. Phys.–Semicond.* **22** 377; *Solid State Commun.* **65** 1189
[19] Ma Y, Fletcher R, Zaremba E, D'Iorio M, Foxon C T and Harris J J 1991 *Phys. Rev.* B **43** 9033
[20] Fletcher R, Zaremba E, D'Iorio M, Foxon C T and Harris J J 1990 *Phys. Rev.* **41** 10 649
[21] Hurley D C 1987 *PhD Thesis* University of Illinois
[22] Xu W, Peeters F M and Devreese J T 1991 *Phys. Rev.* **43** 14 134
[23] See e.g.,
Seeger K 1973 *Semiconductor Physics* (New York: Springer)
[24] Mahan G D 1972 *Polarons in Ionic Crystals and Polar Semiconductors* ed J T Devreese (Amsterdam: North-Holland) p 553
[25] Xu W, Peeters F M and Devreese J T 1993 *J. Phys.: Condens. Matter* **5** 2307
Lei X L 1984 *J. Phys. C: Solid State Phys.* **30** 8
[26] Xu W and Mahanty J 1994 *J. Phys.: Condens. Matter* **6** 4745
[27] Lei X L, Birman J L and Ting C S 1985 *J. Appl. Phys.* **58** 2270
[28] Leadley D R, Nicholas R J, Xu W, Peeters F M, Devreese J T, Singleton J, Perenboom J A A J, van Bockstal L, Herlach F, Foxon C T and Harris J J 1993 *Phys. Rev.* B **48** 5457
Kawamura T and Das Sarma S 1992 *Phys. Rev.* B **45** 3612
[29] Manion S J, Artaki M, Emanuel M A, Coleman J J and Hess K 1987 *Phys. Rev.* B **35** 9203
[30] Makiyama K, Kasai K, Ohori T and Komeno J 1992 *Semicond. Sci. Technol.* **7** B248
[31] Xu W, Peeters F M and Devreese J T 1992 *Phys. Rev.* B **46** 7571